Nanotechnology

PAPER

Flexible and stretchable metallic glass micro- and nano-structures of tunable properties

To cite this article: Haijie Xian *et al* 2019 *Nanotechnology* **30** 085705

IOP Publishing Nanotechnology
Nanotechnology 30 (2019) 085705 (9pp) https://doi.org/10.1088/1361-6528/aaf538

Flexible and stretchable metallic glass micro- and nano-structures of tunable properties

Haijie Xian[1,2], Ming Liu[1,2], Xiaochen Wang[1,2], Fangfu Ye[1,2], Ping Wen[1], Haiyang Bai[1,2,3], Yanhui Liu[1,2,3,4] and Weihua Wang[1,2,3,4]

[1] Institute of Physics, Chinese Academy of Sciences, Beijing 100190, People's Republic of China
[2] University of Chinese Academy of Sciences, Beijing 100049, People's Republic of China
[3] Songshan Lake Materials Laboratory, Dongguan, Guangdong 523808, People's Republic of China
[4] Beijing Advanced Innovation Center for Materials Genome Engineering, Institute of Physics, Chinese Academy of Sciences, Beijing 100083, People's Republic of China

E-mail: yanhui.liu@iphy.ac.cn

Received 31 July 2018, revised 20 November 2018
Accepted for publication 30 November 2018
Published 28 December 2018

Abstract

Flexible and stretchable nanostructures have broad technological applications. Although nanostructures synthesized with metallic glasses, the alloys being of amorphous atomic structure, exhibit superior properties, they are typically too rigid to be used as flexible materials with existing synthesis techniques. In this study we report periodic and crumpled metallic glass nanostructures that can accommodate a large amount of stretching. We demonstrate that their morphologies and characteristic length scale can be well controlled, and that feature sizes as small as ~200 nm can be readily achieved. With their integrity maintained, the nanostructures can be stretched to a strain of ~100%, leading to broadly tunable properties. The approach is not limited to specific metallic glasses, but is applicable to a wide range of glass-forming alloys. This not only enables metallic glasses to be used under extreme stretching conditions, but also helps in the exploration of new functionalities of glassy materials.

Supplementary material for this article is available online

Keywords: metallic glasses, stretchability, flexibility, nanostructures

(Some figures may appear in colour only in the online journal)

Introduction

Metallic nanostructures are of broad technological usefulness, in particular for actuators, detectors, biomedical sensors, fuel cells, and electronic and optical devices [1–3]. The realization of functionality of the nanostructures is highly dependent on how precisely their compositions, atomic structures, and morphologies can be controlled [4]. For conventional crystalline alloys, such controllability is often impeded by the presence of defects, such as dislocations, grain boundaries, and the precipitation of undesired phases [2]. Metallic glasses (MGs) are of homogeneous and isotropic amorphous structure and chemical composition, from macro- down to nanoscale [5–7]. In the amorphous structure, defects such as dislocations and grain boundaries are absent [5], making MGs ideal materials for designing nanostructures of a desired functionality. Furthermore, MGs can be formed in a broad range of compositions, providing abundant choices of tunable properties and functionalities [8].

Owing to their excellent combination of electrical conductivity, large elastic limits and extremely low temperature coefficients of resistance compared with conventional alloys, graphene, and conducting polymers, MGs have been shown to be promising strain-sensing materials in wearable devices, such as electronic skin [9]. In such an application, stretchability is essential because of the large deformability required in order to accompany the movements of the human body.

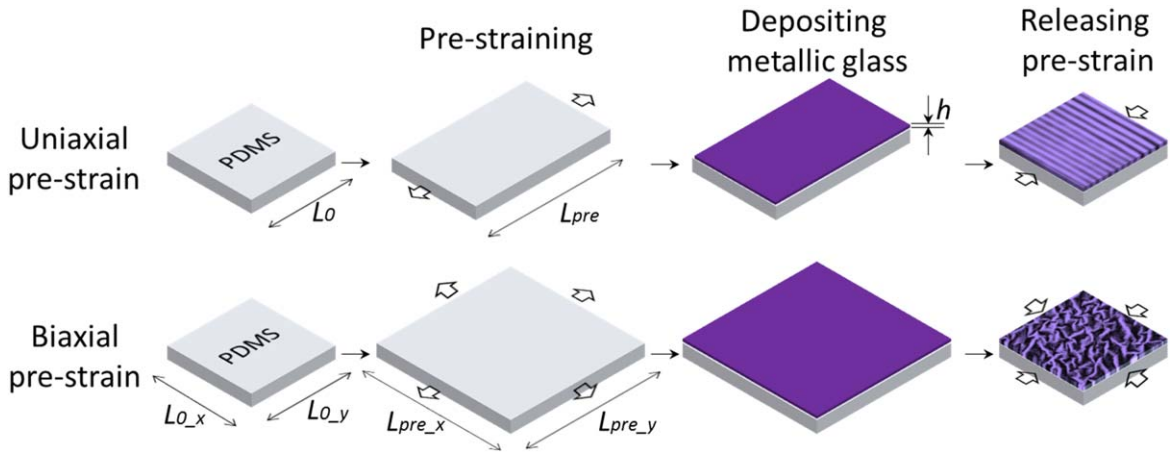

Figure 1. Schematic illustration of the folding approach for NMG fabrication. The PDMS substrates are first stretched uniaxially (upper panel) or biaxially (lower panel) to a pre-strain. Metallic glass films are then deposited on the stretched substrates. Subsequently, the film-coated substrates are released along the pre-straining direction, leading to formation of periodic wrinkle or crumpled wrinkle structures.

At the nanoscale, MGs exhibit a significantly increased elastic limit [10], plasticity, and a remarkable change of electrical resistance with strain [9, 11]. In addition, by forming artificial structures, MGs are capable of accommodating large deformations [12, 13]. These indicate that nanostructured metallic glasses (NMGs) can be better candidates for applications involving stretchable and flexible conditions. However, current approaches to the synthesizing of NMGs via thermal plastic nanomolding [14–17] or oblique angle deposition [18] prevents them from being stretched. Because the NMGs are often supported by rigid substrates [14, 18] that cannot accommodate a high level of lateral strain, failures such as the fracture or delamination of NMGs on the substrates may occur upon stretching [18]. Furthermore, the synthesized NMGs are usually discrete [15, 17–19]. At large lateral deformations, the integrity of the NMGs can be destroyed, leading to degradation or even complete loss of functionality. To circumvent such limitations, continuous NMGs are required.

Surface wrinkling, exhibiting multiple characteristic length scale, is a widely known phenomenon and appears almost everywhere in nature [20, 21]. Inspired by this, a folding approach was proposed and endows plenty of materials for mechanical analysis and emerging applications [22, 23]. According to previous investigations, while metals themselves are not intrinsically stretchable, they can accommodate a significantly greater strain once certain geometrical structures are introduced, to the extent that their use is made possible in soft electronics [24–27]. This suggests that one can obtain superb flexibility and stretchability with MGs by incorporating pre-designed structures.

In this paper, we created ultra-stretchable and flexible NMGs by folding MG films on pre-strained soft substrates. The approach has been successful with pure metals and graphene but not with MGs. We demonstrate that the morphologies and characteristic length scales of the formed structures can be well tailored by the film thickness and the pre-strain applied on the substrate. Through the folding approach, NMGs with characteristic structures and with ridges as small as ~200 nm can be readily achieved with a wide range of MGs, including marginal glass formers. Upon stretching, the NMGs are able to accommodate strains as large as ~100% without damage to their integrity, leading to functionalities that are broadly tunable.

Results and discussion

To fabricate NMGs, we first uniaxially or biaxially stretched the polydimethylsiloxane (PDMS) substrates (figure 1) to different pre-strains, $\varepsilon_{pre} = (L_{pre}–L_0)/L_{pre}$, where L_{pre} is the pre-strained length, and L_0 is the initial length, followed by deposition of MG films. The PDMS substrates were then released from their pre-strained states to the initially unstrained states (figure 1). In this process, the MG films shrank along with the PDMS substrates, leading to macroscopic lateral reduction of the films by the same ratio as that of the substrates. Due to the compressive strain, ε_{pre}, exerted on the film upon substrate shrinking, microscopic wrinkles or crumpled structures formed in the films, arising from folding and buckling. Both the as-deposited and shrunk films were confirmed to be amorphous (figure S1 is available online at stacks.iop.org/NANO/30/085705/mmedia).

We synthesized NMGs by using $Cu_{50}Zr_{50}$ MG, a glass former that is difficult to use for pattern formation with existing methods because of its low oxidation resistance [28] and limited thermal stability [29]. Figure 2 presents the structures formed by uniaxially shrinking the substrates, figure 2(a) with a varying film thickness, h, but constant pre-strain, ε_{pre}, applied on the substrates, and figure 2(b) with a varying ε_{pre} but constant h. As can be seen, uniaxially shrinking the substrates generates nearly periodical wrinkles in the MG films. Height imaging by atomic force microscopy indicates that the wrinkles are quasi-sinusoidal (figure S2). In a previous study, periodic structures of MGs were synthesized by thermal plastic molding [30]. With the folding approach, the expensive and tedious mold fabrication by photolithography and etching of silicon is not needed. Furthermore,

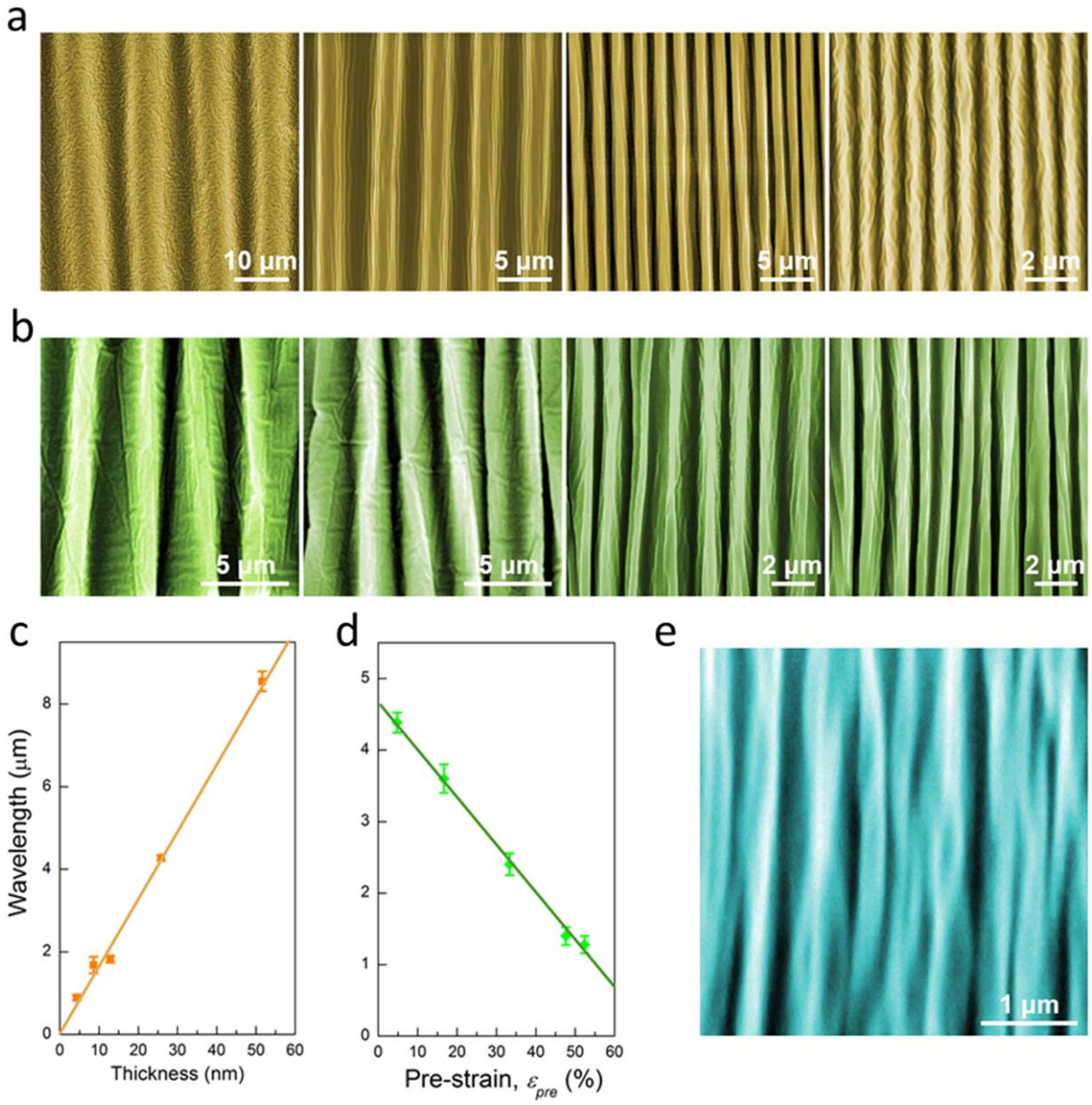

Figure 2. (a) Variation of wrinkles with initial film thickness at a constant pre-strain (30%) of the PDMS substrates. From left to right, the thicknesses are 60 nm, 30 nm, 10 nm, and 5 nm. (b) Variation of wrinkles with pre-strain applied on the PDMS substrates. The thickness of as-deposited films is 16 nm. From left to right, the pre-strains are 17%, 33%, 48%, and 52%. (c) Wrinkle wavelength as a function of film thickness at constant pre-strain. The error bars represent a standard deviation of 5 measurements. Some error bars are smaller than symbols. (d) Wrinkle wavelength as a function of pre-strain at constant film thickness. (e) Nanoscaled wrinkle structure obtained with a film 3 nm thick at a pre-strain of 50%.

it is not necessary to expose the MGs to high temperatures that may result in oxidation or crystallization [7]. In addition, unlike oblique angle deposition which requires pre-patterned templates leading to a shadowing effect and thus discrete nanostructures [18], the structures formed by folding the originally flat MG films are continuous and integrated.

Depending on the initial film thickness, h, and pre-strain of the substrate, ε_{pre}, the wrinkle wavelength λ in the present study can vary by over one order of magnitude, e.g. from $\sim$10 μm down to $\sim$800 nm, while the amplitude of the wrinkle structure can vary by a factor of three, from 250 nm to 750 nm. The largest aspect ratio (defined as the amplitude divided by half of the wrinkle wavelength) of the continuous wrinkle structures is approximately 1, comparable to that of the periodical structures formed by thermal plastic molding [30, 31]. Above the sinusoidal wrinkles, irregular patterns of much smaller size were also found (figure S3), which may originate from residual stress built up or modification of substrate surfaces during deposition, as they can also form during deposition on a PDMS substrate without any pre-strain (figure S3). It is known that the level of residual stress during deposition depends on the material and sputtering conditions [32]. The presence of these small patterns suggests that with the folding approach, the spontaneous formation of hierarchical structures desired in many applications is possible, and tunable by controlling sputtering conditions during film

deposition. As a result of the Poisson effect, cracks perpendicular to the wrinkle were observed (figure S4). For flexible electronics, such cracks can be engineered to be useful.

Figure 2(c) plots the wrinkle wavelength λ as a function of the initial film thickness, h. The wrinkle wavelength was obtained by averaging 20 continuous wrinkles from different regions. Within the range under investigation, the wrinkle wavelength appears to be linearly proportional to the initial thickness of the deposited MG film. Although the smallest wrinkle wavelength in figure 2(a) is ~800 nm when h equals ~5 nm, the tendency revealed by the λ versus h plot suggests that wrinkles of smaller wavelength can be achieved with thinner MG films. It should be mentioned that the pre-strain used to create those wrinkle structures is only ~29%. With PDMS, a pre-strain of more than 50% is readily obtainable. Figure 2(b) illustrates the variation of wrinkle structures with increasing pre-strain while maintaining film thickness constant, e.g. $h = 16$ nm. It is evident that an increment of pre-strain results in a significantly reduced wrinkle wavelength, and wrinkles of wavelength as small as ~1 um can be obtained when the pre-strain reaches a high value of ~50%. As shown in figure 2(d), the plot of wrinkle wavelength λ as a function of pre-strain ε_{pre} indicates that λ is linearly dependent on ε_{pre}. From figures 2(c) and (d), it is evident that the wrinkle structures can be controlled by either film thickness or pre-strain applied on the PDMS substrate, by which a wide range of wrinkle wavelengths can be achieved. In figure 2(e) we show that wrinkle structures of wavelengths as small as 300 nm can be readily realized when the initial film thickness is ~3 nm and pre-strain ε_{pre} in the PDMS substrate is ~ 50%. In our work, the local deformation of the metal layer is estimated to be ~0.7%, which is beyond the elastic limit of crystalline metals, so plastic deformation may occur in the wrinkled structures. However, the elastic limit for metallic glass is as large as ~2% [33]. This may explain why the wavelength decreases faster with pre-strain, compared with previous studies (figure S5) [34, 35].

In addition to the wrinkle structures formed by uniaxial pre-straining and shrinking, more complex structures are also possible by biaxially shrinking the substrates. Figure 2 illustrates crumpled wrinkles formed by simultaneously releasing PDMS from a pre-strained state along two directions (figure 1). Unlike the periodicity of wrinkles upon uniaxial shrinking, biaxial shrinking leads to quadrangular-like patterns with the crumpled wrinkles appearing as ridges. The length scale of the patterns also relies on the film thickness h and the pre-strain ε_{pre} (figure 3). With an increase in film thickness h, the length scale of the quadrangular-like patterns increases (figure 3(a)), while an increased pre-strain, ε_{pre}, of the PDMS substrates reduces the pattern sizes to smaller values (figure 3(b)). In both cases, the patterns and the ridges are continuous. Since the distribution of the pattern sizes is not as uniform as that of the wrinkle structures formed by uniaxial shrinking, we quantify the characteristic length scale of the patterns as the following. We first identify the ridges that appear to be brighter in scanning electron microscopy (SEM) images, so that the quadrangular-like patterns can be isolated. The average area of the patterns was converted to an equivalent mean diameter, d, as a characteristic size of the patterns. Figures 3(c) and (d) display d versus h, and d versus ε_{pre} ($\varepsilon_{pre\_x} = \varepsilon_{pre\_y}$), respectively. As can be seen, within the range of the present study, d appears to linearly decrease with the reduction of film thickness h (figure 3(c)) and an increase of the pre-strain applied on the PDMS substrates, ε_{pre} (figure 3(d)). At the same time, the width of the ridges also decreases (figures 3(a) and (b)). These relationships indicate that the characteristic length scales of the crumpled wrinkles can be tuned by varying h and ε_{pre}, which leads to the formation of NMGs and crumpled wrinkles. On average, the ridge width can be as small as 200 nm (figure 3(e)). In addition to uniaxial and biaxial pre-straining of the substrates, radial pre-straining leads to patterns that appear to be more random (figure S6), suggesting the versatility of the method in the fabrication of surface structures.

Because the NMGs are continuous and created on stretchable substrates, they are thus flexible and able to be stretched along the pre-straining directions of the substrates. For example, we have stretched the NMGs up to a strain, ε, as large as ~100% ($\varepsilon = (L_1–L_0)/L_0$, where L_1 is the lateral length of the NMGs upon stretching and L_0 their initial length). After being released back to their initial lateral dimension, the crumpled wrinkle NMGs can maintain their initial morphologies and characteristic length scale (figures 4(a) and (b)). At the same time, the sample can be bent or twisted (see the insets of figures 4(c) and (d)), illustrating the excellent flexibility of the NMGs. After the bending and twisting test, there was no observable change in the continuity or integrity of the structure (figures 4(c) and (d)). Moreover, no delamination of the structures from the substrate was observed (figure S4), suggesting excellent adhesion between the MG film and a PDMS substrate.

Upon stretching, the NMGs unfold towards their initially flat state. Accompanying this unfolding process is the variation of transparency of the NMGs. Despite that, the NMGs appear to be opaque in the as-prepared state (figure 5(a)). Owing to the absorption of incident light by the structures, they gradually become transparent to human eyes and the characters underneath the NMGs become visible with increasing stretching strain (figure 5(b)). To quantitatively evaluate the variation of transparency, we measured the transmittance spectra for the NMGs stretched to different strains. Figure 5(c) displays the change of transmittance spectra of a wrinkle NMG with uniaxial stretching. As can be seen, with increasing stretching strain, ε, the spectra gradually shift upwards to a higher transmittance, suggesting better transparency. To reveal the tendency of the variation, we identify the transmittance values at a constant light wavelength, e.g. 700 nm, and plot them as a function of ε. As shown in figure 5(d), the data points follow well an exponential equation due to a decay of intensity of electromagnetic wave while going through the materials. The low transparency of the sample under a small stretching can be attributed to light absorption by the NMGs (figure S7), because the measured reflectivity of the sample is negligible (figure S8). This implies that the NMGs have great potential in strain sensor applications with transmittance as sensing signals, and

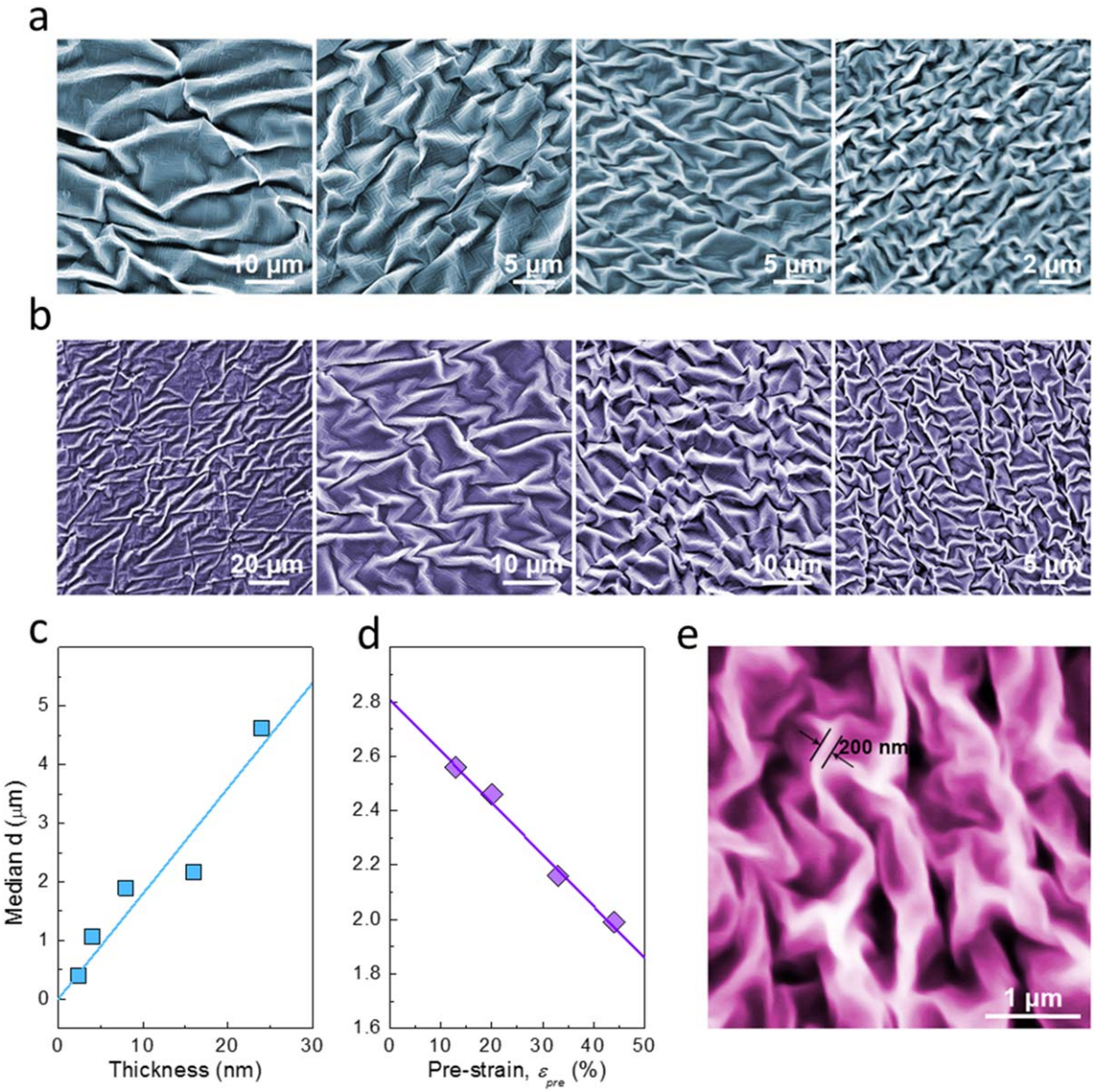

Figure 3. (a) Variation of crumpled wrinkles with initial film thickness at constant pre-strain $\varepsilon_{pre\_x} = \varepsilon_{pre\_y} = 33\%$ applied on the PDMS substrates. From left to right, the thicknesses are 24 nm, 16 nm, 8 nm, and 4 nm. (b) Variation of the formed structures with pre-strain $\varepsilon_{pre\_x} = \varepsilon_{pre\_y}$ applied on the PDMS substrates. The thickness of the as-deposited glassy films is 16 nm. From left to right, the pre-strains are 13%, 20%, 33%, and 44%. (c) Equivalent diameter d versus initial film thickness at constant pre-strain. (d) d vs. pre-strain at constant film thickness. (e) NMGs obtained with a film 3 nm thick at a pre-strain of $\varepsilon_{pre\_x} = \varepsilon_{pre\_y} = 43\%$.

the sensible strain can be as high as 80%, an order of magnitude larger than that with MG fibers (<2%) achieved with their piezoresistance effect [11].

Thanks to the high stretchability of the micro- and nano-structures, transition in wettability can be realized by tuning the length scale of the formed structures. Figure 6 shows variation of contact angle upon the stretching–unstretching cycle exerted on a crumpled structure of a characteristic size of ~600 nm. Before straining, the sample exhibits typical hydrophobic behavior featured by a contact angle of 112.8°. The transition from hydrophobicity to hydrophilicity can be observed when the structure is stretched to a strain of ~25%. Further stretching results in an even smaller contact angle. At the maximum achievable strain, ~50% for this sample, the contact angle decreases to a value of 72.3°, consistent with that for the $Cu_{50}Zr_{50}$ MG of flat surface. Upon unstretching, the crumpled structure flattened upon stretching reforms, and the wettability changes from hydrophilicity to hydrophobicity, characterized by the increasing contact angle, from 72.3° back to 111.9°. It can be seen that the variation in wettability is approximately linear upon both stretching and unstretching, and the absolute slopes are almost the same, indicating a convenient approach for tuning the wettability of MG films.

In addition to achieving tunable light transmittance and wettability, the micro- and nano-structures can also be used to modulate cell behaviors. To demonstrate this, we cultured mammary cyst cells (MCF 10 A) on flat MG film and a wrinkle structure of wavelength of 4 μm. As can be seen in figure 7(a), the MCF 10 A cells tend to form aggregates on the

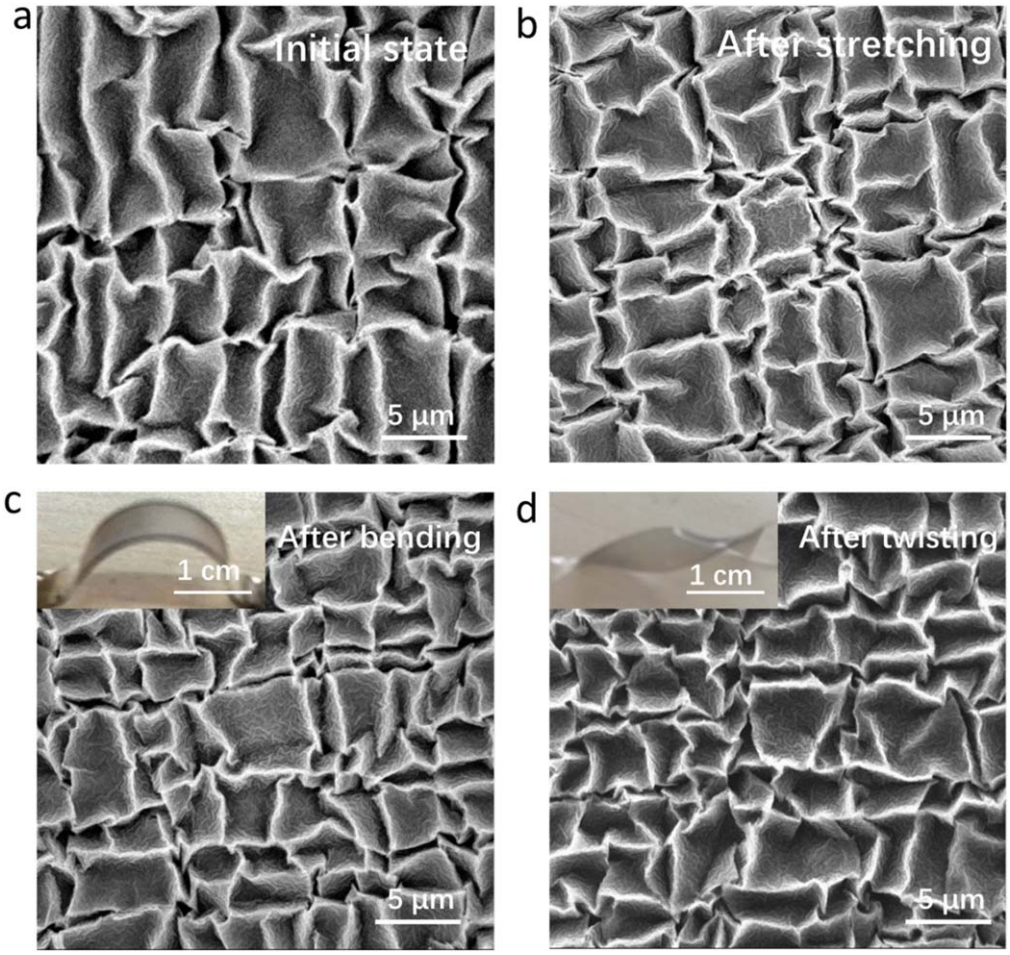

Figure 4. Flexible and stretchable metallic glass crumpled structures. (a) SEM images of crumpled structure before cyclic stability test. (b) SEM images of crumpled structure after stretching up to strain $\varepsilon = (L_1–L_0)/L_0 = 100\%$ more than 100 times. (c), (d) are SEM images of the sample after 100 bending and twisting tests, respectively. Inserts are optical images of the sample in bending and twisting states. The initial thickness of MG film is 18 nm, and $\varepsilon_{pre\_x} = \varepsilon_{pre\_y} = 55\%$.

flat MG film. The orientation of the cells appears to be random (figure 7(c)). However, the cells cultured on the wrinkle structures distribute evenly on the sample (figure 7(b)), and no cell aggregates can be observed. Compared with that on the flat MG film, there are far fewer cells being attached to the wrinkle structure, and the cells that do attach to the structures are elongated along the valley of the wrinkles (figure 7(c)). The results indicate that the wrinkle structures have substantial influence on cell behaviors and can be incorporated in the design of biomaterial surfaces for biomedical devices. In comparison with the crease patterns of low aspect ratio by polymer, MG patterns with high aspect ratios can better restrict cell movement [36, 37]. Furthermore, the conductivity of MGs implies that an external field can be applied to study cell electrophoresis.

As we have demonstrated above, the folding approach is highly controllable and the structures formed are easily tunable. The dominant parameters that govern the characteristic length scale of the NMGs are the film thickness and the pre-strain applied on the substrate. The approach is not limited to bulk glass formers. Instead, it can be a general method applicable to a broad range of MGs. Deposition is known to experience a high effective cooling rate of the order of 10^9 K s^{-1} [38]. Under such a high cooling rate, a wide range of alloys including marginal glass-forming alloys can form glassy films. The limitation is whether an alloy can reach a glassy state under such a cooling rate, or the glass-forming ability of the alloy. Since heating to a high temperature is not required with the folding approach, NMGs of alloys of marginal glass-forming ability can retain their amorphous nature during fabrication. For example, we have synthesized periodic and crumpled wrinkle structures with $Fe_{78}Si_9B_{13}$ MG, which is an alloy of limited thermal stability and glass-forming ability, but which has broad applications due to its soft magnetic property (figure S9).

In addition to continuous micro- and nano-structures, such as periodic wrinkles or crumpled wrinkles, discrete patterns in NMGs can also be realized if the PDMS substrates are pre-patterned prior to film deposition, or the substrates are covered by shadow masks during film deposition. A variety of pre-patterning techniques such as optical or electron-beam lithography have been well established and shadow masks of various structures are available [39]. To demonstrate the discrete NMG patterns, we use copper mesh as shadow masks. As shown in figure 8, the discrete NMG patterns are well aligned, completely inheriting the patterns of copper

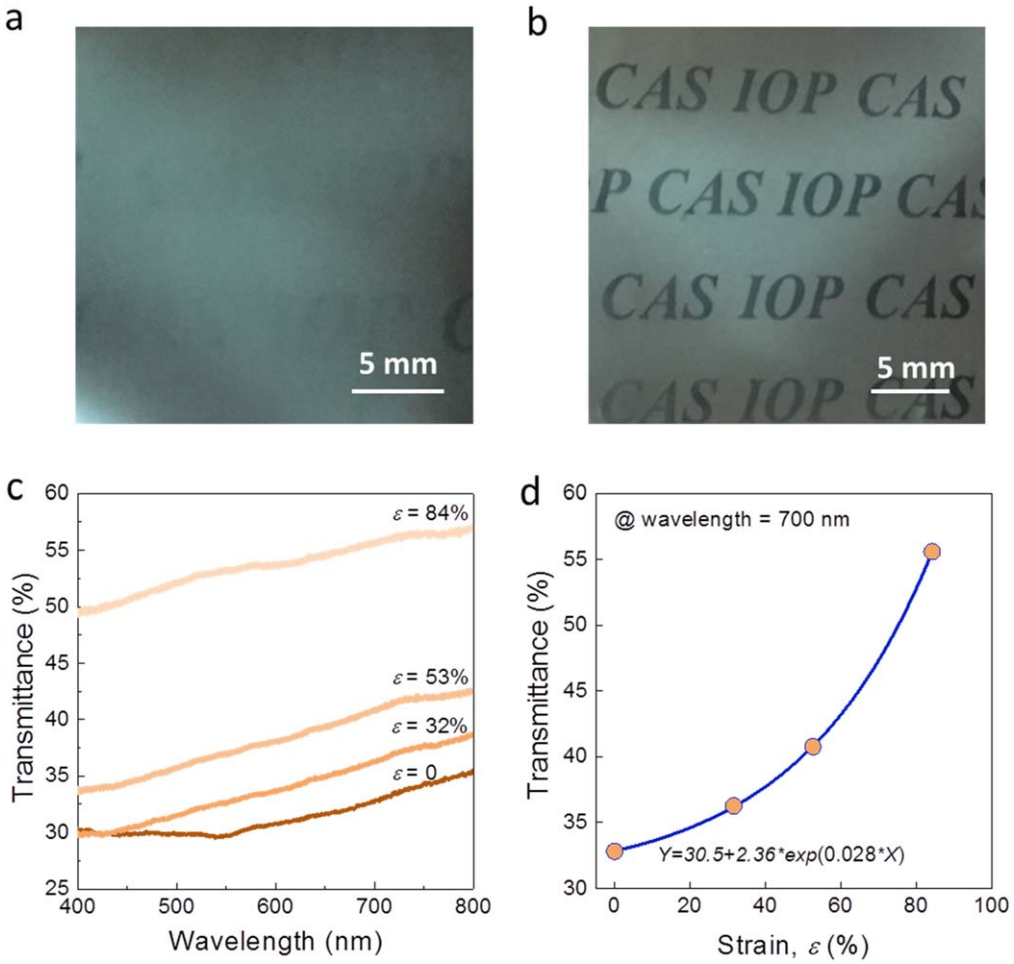

Figure 5. Optical images of a NMG before (a) and after (b) biaxial stretching. The NMG was synthesized with 24 nm thick film. (c) Transmittance spectra of NMGs at different stretching strains $\varepsilon = (L_1 - L_0)/L_0$ in the wavelength range of 380–800 nm. The NMGs were synthesized with 15 nm thick film. (d) Variation of transmittance with strain at a wavelength of 700 nm.

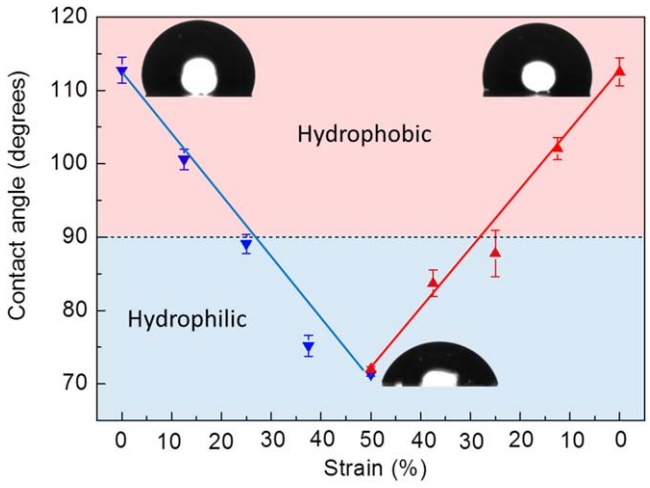

Figure 6. Water contact angle as a function of biaxial stretching strain for a crumpled structure of characteristic size of 600 nm. The inserts are images showing a water droplet at different stretching strains. The initial thickness of the MG film is 4 nm.

mesh. The sizes, shapes, and spacing of the NMG patterns can thus be well manipulated by that of pre-patterns or shadow masks. Similar to the continuous NMGs, the characteristic length scale of the discrete NMGs is a function of the initial film thickness and the pre-strain applied on the substrate.

Conclusion

In summary, we have demonstrated a rapid and versatile folding approach that can generate a wide variety of ultra-stretchable NMGs with a characteristic length scale ranging from a few microns down to a couple of hundred nanometers. The parameters that govern the formation of such structures include the thickness of the deposited metallic glass films, and the direction and amount of pre-strain, all of which are convenient to control, so that the formed NMGs are highly tunable. More importantly, the NMGs synthesized via the folding approach exhibit excellent flexibility, ultra-large stretchability, and remarkable robustness, demonstrating their potential use as flexible materials. We further demonstrated that the optical transmittance, wettability, and cell behaviors can be modulated with the structures. Since the folding approach can be used for a wide range of alloy compositions that can form glass, the broadly tunable morphologies of the NMGs, along with the far-from-equilibrium thermodynamic

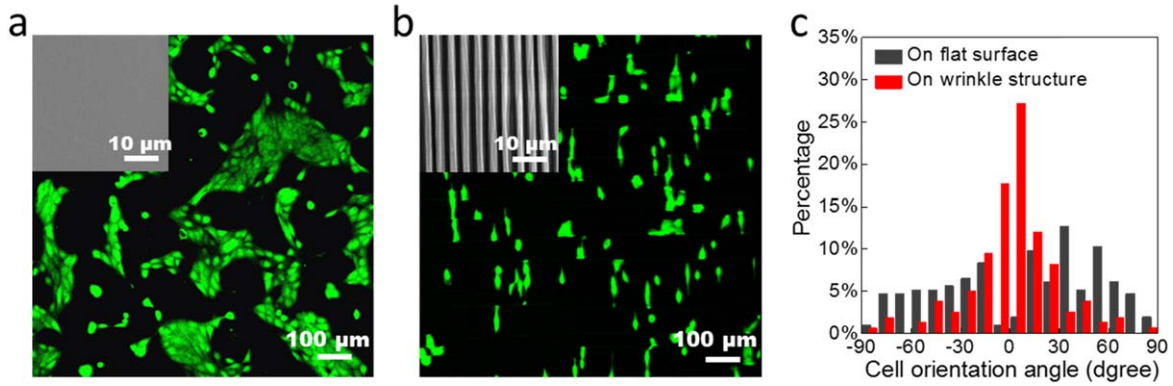

Figure 7. Fluorescent images of MCF 10 A cells on flat (a) and unixial patterned (b) surfaces. The inserts are SEM images of flat MG film and a wrinkled structure of wavelength ~4 μm. (c) Distribution of cell orientation on flat MG film and wrinkled structure. The initial thickness of the films is 24 nm, and pre-strain $\varepsilon_{pre} = 33\%$.

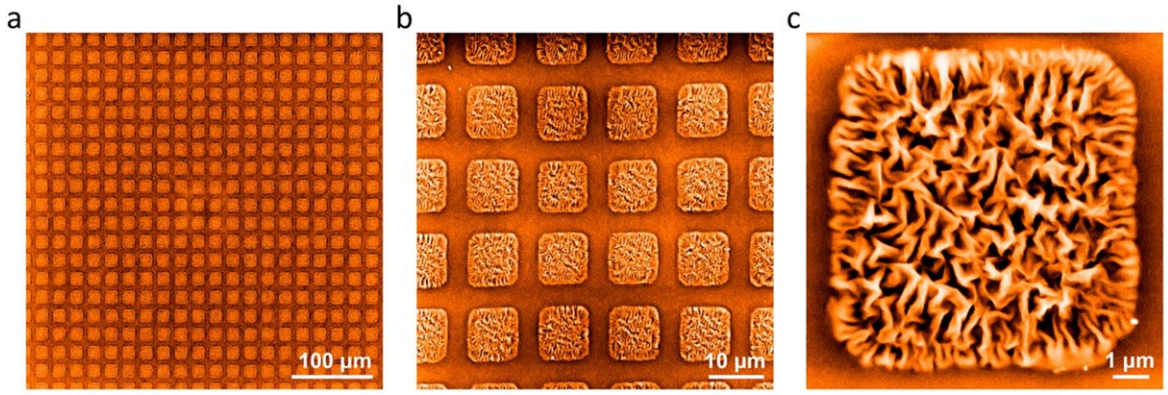

Figure 8. SEM images of discrete NMG pattern. (a) Overview of the NMG pattern. (b) Close-up view. (c) Zoom-in of individual NMG. The pattern was synthesized with a 3 nm thick film and the pre-strain applied on the PDMS substrate was $\varepsilon_{pre\_x} = \varepsilon_{pre\_y} = 33\%$.

states of MGs, are also of importance in exploring other surface-dominated behaviors and properties. Furthermore, due to the absence of defects such as grain boundaries, metallic glasses are much more corrosion-resistant than their crystalline counterparts. This suggests that the surface patterns formed by metallic glasses have potential to be used in harsh environments.

Experimental

Materials fabrication

PDMS substrates were prepared by mixing prepolymer and curing agent (Dow Corning, Sylgard 184) at the weight ratio of 10:1. After degassing in a vacuum chamber, the mixed polymer was cured at 80 °C for 2 h. $Cu_{50}Zr_{50}$ and $Fe_{78}Si_9B_{13}$ MGs were chosen for film deposition. The $Cu_{50}Zr_{50}$ targets were prepared by arc melting pure elements in a Ti-gettered argon atmosphere and then *in situ* suction casting in a Cu mold. The $Fe_{78}Si_9B_{13}$ target was commercial amorphous ribbons from Antai Technology Company. MG thin films were deposited using ion beam deposition. The base pressure before deposition was 1×10^{-4} Pa, and the working argon pressure was 2.4×10^{-2} Pa. The accelerating voltage was 750 eV. The thickness of the films was controlled by adjusting the ion beam current and deposition time.

Materials characterization and property tests

The amorphous nature of deposited films was examined by a Rigaku SmartLab (9 kW) high-resolution x-ray diffractometer and a differential scanning calorimeter (Pekin Elmer DSC8000) at a heating rate of 20 K min^{-1}. The thicknesses of the deposited MG film were measured by x-ray reflectivity (Rigaku SmartLab). Structure and morphology characterizations were performed using a Phenom XL scanning SEM and a MFP 3D Asylum Research atomic force microscope. The transmittance was measured with a grating spectrometer (SP2555, Princeton Instruments, USA) at wavelengths of 380 nm–800 nm. The water contact angle was determined via a Dataphysics OCA20 contact angle system. The water droplet used was about 1 μl. At least three water drops at different locations were measured, and the mean values and standard deviations were calculated to plot each data item in figures. For cell culturing, the samples were first sterilized with 75% ethanol and deionized (DI) water three times and then coated with fibronectin at 5 mg cm^{-2} overnight at 37 °C. After the fibronectin coating was applied, the samples were washed by 1X phosphate buffer saline three times and

incubated at 37 °C for 1 h. MCF-10A cells (American Type Culture Collection) were cultured in a Dulbecco's modified eagle medium/F12 medium containing L-glutamine and 15 mM 4-(2-hydroxyethyl)-1-piperazineethanesulfonic acid (10-092-CVR, Corning) supplemented with 5% horse serum (16 050-122, Gibco), 20 ng ml^{-1} human epidermal growth factor (PHG0311, Gibco), 10 mg ml^{-1} insulin (I-1882, Sigma), 1% penicillin/streptomycin (30-002-CI, Corning), 100 ng ml^{-1} cholera toxin (C-8052, Sigma), and 0.5 mg ml^{-1} hydrocortisone (H-0888, Sigma). Before culturing, the cells were stained by Calcein-AM (green) for 30 min. Images of each sample were taken using a confocal microscope (Leica, SP8) with a 25X water objective. Cell alignment was analyzed by measuring the orientation of cells using ImageJ software. More than 150 cells were analyzed in each sample; 0 degree means the direction parallel to the pattern.

Acknowledgments

We are grateful for experimental assistance from X Zhou, L Q Shen, Y C Wu, P Luo, and S Meng, discussions with Y C Hu, B Wang, Y T Sun, and L Z Zhao, and financial support from NSF of China (Grant Nos. 51571209 and 51461165101), the MOST 973 Program of China (No. 2015CB856800), and the Key Research Program of Frontier Sciences, CAS (QYZDY-SSW-JSC017). Y H Liu acknowledges funding from the Hundred Talents Program, CAS, and the National Thousand Young Talents Program of China.

Conflicts of interest

There are no conflicts to declare.

ORCID iDs

Yanhui Liu https://orcid.org/0000-0002-7546-3371

References

[1] Arico A S, Bruce P, Scrosati B, Tarascon J M and Van Schalkwijk W 2005 *Nat. Mater.* **4** 366–77
[2] Noorduin W L, Grinthal A, Mahadevan L and Aizenberg J 2013 *Science* **340** 832–7
[3] Ding Y and Chen M W 2009 *MRS Bull.* **34** 569–76
[4] Brett M J and Hawkeye M M 2008 *Science* **319** 1192–3
[5] Chen M W 2011 *NPG Asia Mater.* **3** 82–90
[6] Schroers J 2013 *Phys. Today* **66** 32–7
[7] Kumar G, Desai A and Schroers J 2011 *Adv. Mater.* **23** 461–76
[8] Ding S, Liu Y, Li Y, Liu Z, Sohn S, Walker F J and Schroers J 2014 *Nat. Mater.* **13** 494–500
[9] Xian H J *et al* *Appl. Phys. Lett.* 2017 **111** 121906
[10] Tian L, Cheng Y Q, Shan Z W, Li J, Wang C C, Han X D, Sun J and Ma E 2012 *Nat. Commun.* **3** 609
[11] Yi J, Bai H Y, Zhao D Q, Pan M X and Wang W H 2011 *Appl. Phys. Lett.* **98** 241917
[12] Chen S H, Chan K C, Yue T M and Wu F F 2018 *Scr. Mater.* **142** 83–7
[13] Sarac B and Schroers J 2013 *Nat. Commun.* **4** 2158
[14] Liu L C, Hasan M and Kumar G 2014 *Nanoscale* **6** 2027–36
[15] Kumar G, Tang H X and Schroers J 2009 *Nature* **457** 868 - 872
[16] Liu X, Chen N, Gu J L, Yang G N, Mussler G and Yao K F 2015 *Mater. Design* **87** 1018–21
[17] Zhang W, Guo H, Chen M W, Saotome Y, Qin C L and Inoue A 2009 *Scr. Mater.* **61** 744–7
[18] Liu Y H, Liu J B, Sohn S, Li Y L, Cha J J and Schroers J 2015 *Nat. Commun.* **6** 7043
[19] Hasan M, Schroers J and Kumar G 2015 *Nano Lett.* **15** 963–8
[20] Smith S M 2002 *Human Brain Mapping* **17** 143–55
[21] Genzer J and Groenewold J 2006 *Soft Matter* **2** 310–23
[22] Zang J, Ryu S, Pugno N, Wang Q, Tu Q, Buehler M J and Zhao X 2013 *Nat. Mater.* **12** 321–5
[23] Khang D Y, Jiang H, Huang Y and Rogers J A 2006 *Science* **311** 208–12
[24] Lacour S P, Wagner S, Huang Z Y and Suo Z 2003 *Appl. Phys. Lett.* **82** 2404–6
[25] Rogers J A, Someya T and Huang Y 2010 *Science* **327** 1603–7
[26] Dickey M D 2017 *Adv. Mater.* **29** 1606425
[27] Yan W, Page A, Nguyen-Dang T, Qu Y, Sordo F, Wei L and Sorin F 2018 *Adv. Mater.* 1802348
[28] Shi J A, Cao C R, Zhang Q H, Sun Y T, Wang C, Wang W H, Bai H Y and Gu L 2017 *Scr. Mater.* **136** 68–73
[29] Yu P, Bai H Y and Wang W H 2006 *J. Mater. Res.* **21** 1674–9
[30] Chu J P, Wijaya H, Wu C W, Tsai T R, Wei C S, Nieh T G and Wadsworth J 2007 *Appl. Phys. Lett.* **90** 034101
[31] Saotome Y, Imai K, Shioda S, Shimizu S, Zhang T and Inoue A 2002 *Intermetallics* **10** 1241–7
[32] Liu Y H, Fujita T, Hirata A, Li S, Liu H W, Zhang W, Inoue A and Chen M W 2012 *Intermetallics* **21** 105–14
[33] Telford M 2004 *Mater. Today* **7** 36–43
[34] Jiang H, Khang D Y, Song J, Sun Y, Huang Y and Rogers J A 2007 *Proc. Natl Acad. Sci. USA* **104** 15607–12
[35] Song J, Jiang H, Liu Z J, Khang D Y, Huang Y, Rogers J A, Lu C and Koh C G 2008 *Int. J. Solids Struct.* **45** 3107–21
[36] Tung N D, de Luca A C, Yan W, Qu Y P, Page A G, Volpi M, Das Gupta T, Lacour S P and Sorin F 2017 *Adv. Funct. Mater.* **27** 1605935
[37] Wang Q M and Zhao X H 2016 *MRS Bull.* **41** 115–22
[38] Liu Y H, Fujita T, Aji D P B, Matsuura M and Chen M W 2014 *Nat. Commun.* **5** 3238
[39] Lei Y, Yang S K, Wu M H and Wilde G 2011 *Chem. Soc. Rev.* **40** 1247–58